Chapter 9
Sintered Nano-Ag as Joining Material for Thermoelectric Modules

K. Brinkfeldt, J. Simon, K. Romanjek, S. Noel, M. Edwards, J. Räthel, M. Da Silva, and D. Andersson

Abstract The use of sintered silver particles as an alternative to other types of joining materials for the electrical connection between thermoelectric materials and the substrate in thermoelectric modules (TEM) has been investigated. Sintered silver particles have recently gained attention in the field of power electronics due to the high thermal and electrical conductivity of the material. The nanosilver paste used in this work has originally been developed for use as a die attach material, where these properties are important. The sintering process involved a thermal treatment at 310 °C, under a 15 kg mechanical load, in a nitrogen atmosphere. Sample TEMs with sintered silver connections were tested both mechanically and electrically. Initial results showed that the TEMs performed well during thermal gradient tests with the hot side heated from 50 °C to 550 °C and the cold side kept at 20 °C. This performance also indicates that the nano-Ag joints have good contact resistance. The resistivity of the sintered silver joints were measured at room temperature to $\rho = 15$ µΩ m (average value of Ti/Au plated thermoelectric legs). Shear force tests of the sintered thermo electrical leg material showed that the joints are brittle when W metallized AlN substrates were used and these have an average shear strength of 3.3 ± 1.9 MPa. On Cu metallized AlN substrates, ductile fracture behavior was observed and an average shear strength of 2.4 ± 1.4 MPa was measured.

Keywords Thermoelectric modules • Joining material • Contact resistance • Shear force • Nanosilver

K. Brinkfeldt (✉) • M. Edwards • M. Da Silva • D. Andersson
Swerea IVF, Argongatan 30, 431-53 Mölndal, Sweden
e-mail: klas.brinkfeldt@swerea.se

J. Simon • K. Romanjek • S. Noel
CEA, 17 rue des Martyrs, 38054 Grenoble Cedex 9, France

J. Räthel
Fraunhofer IKTS, Winterbergstrasse 28, 01277 Dresden, Germany

A. Amaldi and F. Tang (eds.), *Proceedings of the 11th European Conference on Thermoelectrics: ECT 2013*, DOI 10.1007/978-3-319-07332-3_9,
© Springer International Publishing Switzerland 2014

Introduction

Thermoelectric (TE) materials rely on the Seebeck effect to transform heat energy to electric power. Due to their simple, reliable operation without moving parts they have been deployed as part of the power generation in space applications for several decades [1–3]. They are also under investigation as waste heat recovery devices in industrial and automotive applications [4–6].

Though the efficiency of the TEM depends largely on the properties of the TE-material itself, the properties of the interface and electrode materials are also important. If the joining and current-carrying materials do not have high thermal and electrical conductivities, the efficiency is decreased due to resistive losses. The interface materials are also critical from a reliability perspective. As applications of TE-modules (TEMs) involve high temperature gradients, thermal cycling, or both, difficulties arise due to the coefficient of thermal expansion (CTE) mismatches between the constituent materials, resulting in significant stresses and strains, which ultimately could cause fracture in the interface.

Others have recently reported on the use of Ag–Cu brazing methods to join $CoSb_3$ and Cu [7]. $CoSb_3$-based skutterudite materials have also been joined with Mo or Mo–Cu electrodes by spark plasma sintering using Ti or Ag–Cu foils [8–10]. Kadhim et al. have used Ag-paste/Cu plate/Ag-paste as electrodes for Bi–Sb–Se–Te and Bi–Se–Te TE-materials [11]. They conclude that the contact resistance R_c is mostly attributed to the boundary resistance and the contribution of the Ag–Cu–Ag electrodes is very small. The details of the Ag paste were not reported.

Recently, sintered nano-Ag particles have been introduced as a die attach material in the field of power electronics [12]. The material consists of nanoscale particles in an organic solvent/binder. The small particle size enables a sintering temperature in the order of 250–310 °C depending on if the surface material is Ag or Au, while the resulting joint is pure Ag with a melting temperature, $T_m = 961$ °C. Chen et al. reported that nano-Ag can have similar or improved mechanical properties compared to solder joints [13]. This, combined with the high thermal and electrical conductivity of Ag, low processing temperature and high T_m, makes the material very attractive to power electronics die attach applications, which also makes it attractive to use in TEMs.

In this work we have evaluated nano-Ag as the joining material in small, proof of concept TEMs consisting of four SiGe TE-legs joined to ceramic substrate metallizations of different materials. In “Method” section, the fabrication of samples, including the SiGe TEMs and special samples used for contact resistance (R_c) measurements, are described. Two different metallizations schemes for the SiGe TE-legs were investigated with respect to contact resistance: Ti/Au and MoSi2/Ti/Ag. “Method” section also describes the measurement setups for the electrical and mechanical tests. “Result” section describes the results of the R_c measurements, mechanical test, and performance of the TEMs during thermal gradient tests with ΔT ranging from 30–530 °C.

Method

Sample Manufacturing Process

The TE material used in all of the measurements in this work was a polycrystalline Silicon–Germanium alloy (80 % Si and 20 % Ge) made by spark plasma sintering, with mechanical synthesis of the initial powder [14]. The material is completely dense and has a submicron scale grain size. The N-type dopant is Phosphorous and P-type is Boron.

The TE-material was sintered into pellets, which were then metallized on top and bottom. Two different metallizations: (a) thin Ti/Au and (b) $MoSi_2$/Ti/Ag were used, and the pellets were then diced into $4 \times 4 \times 5$ mm^3 TE-legs. For metallization (b), $MoSi_2$ was included as a barrier material. The use of silicides as diffusion barrier materials has shown good results in thin film applications at very high temperatures [15–17]. The $MoSi_2$ layer was created by sputtering a thin Mo layer followed by a thin Si layer and this was repeated 60 times to create a film of the desired thickness. The sputtering times were calibrated, so that the ratio of Mo atoms to Si atoms was as close as possible to 0.5. This layered sputtering step was followed by an annealing step at 900 °C for 3 h. After annealing, the resulting $MoSi_2$ layer was $\approx$90 nm thick. Finally, the $MoSi_2$ layer was covered with a Ti/Ag capping layer (Ag thickness $\approx$2 μm).

The TE-legs (two P-type and two N-type) were then sintered to cold and hot side substrates to form proof of concept TEMs. The types of metallizations used on the different TEM substrates are listed in Table 9.1.

The nano-Ag material used to sinter the TE-legs to the substrate metallizations was nanoTach paste from NBE-Tech, Virginia. Nano-Ag was selected due to its high thermal and electrical conductivity, as well as its low Young's modulus compared to Cu.

The process to make the connection involved screen-printing of the nano-Ag paste onto both hot and cold side substrate metallizations, the TE-legs were then attached to the hot and cold side metallizations, which was followed by a sintering process in a furnace at 310 °C with or without pressure applied at the peak temperature. The peak temperature (and pressure, when used) was maintained for 20 min. The resultant joining interface is able to operate at much higher temperatures, which

Table 9.1 Substrates and metallizations used in the TEMs

Substrate	Material	Metallization
AlN/Cu Cold side	AlN	300 μm Cu/0.1 μm Au/10 μm nano-Ag/300 μm Ag
AlN/Cu Hot side	AlN	300 μm Cu/0.1 μm Au
AlN/W Cold side	AlN	16 μm porous W/10 μm Ni/0.1 μm Au/10 μm nano-Ag/300 μm bulk Ag
AlN/W Hot side	AlN	16 μm porous W/10 μm Ni/0.1 μm Au

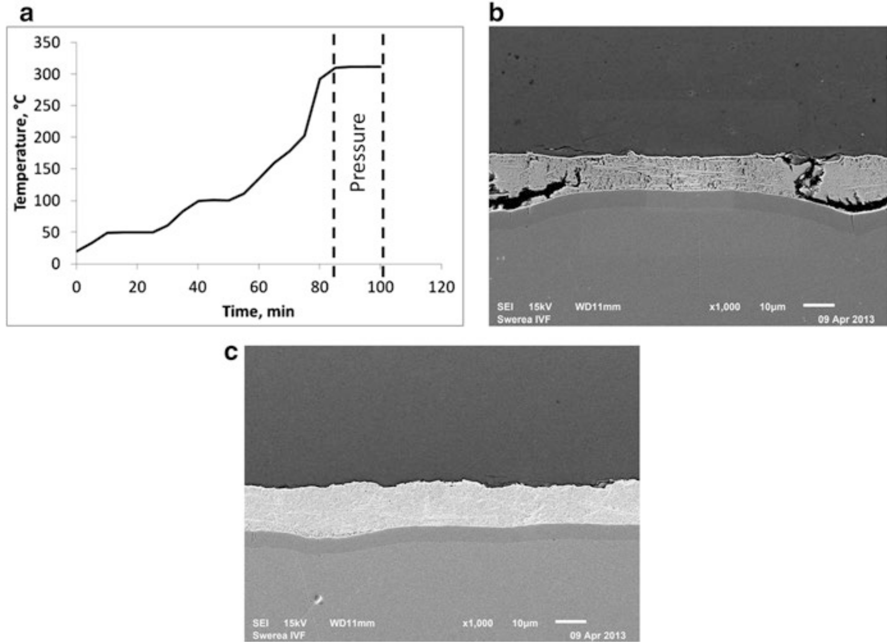

Fig. 9.1 (**a**) Measured temperature profile for nano-Ag sintering process. (**b** and **c**) SEM images of the cross section of SiGe leg material sintered to a Cu surface. The image (**c**) shows the resulting interface with pressure applied during the final processing step

are theoretically near the melting temperature of Ag at $T_m = 961$ °C, if the joint itself is not required to withstand mechanical loads.

Figure 9.1 shows the measured temperature profile for the nano-Ag sintering process in a N_2 atmosphere. If the bond surfaces are large, then an additional mechanical pressure during the final temperature step is required. Since the TE-leg surface area is 4×4 mm^2, which is close to the limit, tests with and without mechanical pressure have been made. Figure 9.1 also shows comparative cross sections of SiGe TE-legs sintered to a Cu surface using nano-Ag paste. The sample in Fig. 9.1c has been sintered with a mechanical load of 15 kg applied during the final sintering step. This load corresponds to a pressure of ≈2–3 MPa on the sintered interfaces. This process was followed by a slow, passive cooling period for several hours. When the temperature decreased below 70 °C, the furnace was opened and the remainder of the cooling was done in air.

Electrical Measurement Setup

A 4-point resistance (R4P) measurement method was used to find the total resistance of the TEM. A known current was forced through the TEM and the voltage was measured between the input and output. The resistance through the TEM was

then calculated using Ohm's law. The measurements were done at room temperature and the device is assumed to be passive (zero heat flux through the device). In order to limit the Peltier effect, which appears when a current is forced through a TEM, currents were limited to −100 mA–100 mA and the U(I) characteristics were measured for less than 1 s.

The measurement principle used to determine the contact resistance (R_c) of the nano-Ag interface was similar. Special samples were prepared for this measurement. Two TE-legs, consisting of the same N- or P-type material, were attached directly to each other using the nano-Ag sintering process. Current was then forced between the top and the bottom of the TE-leg/joint/TE-leg stack and the voltage was measured on either side of the joint. The resistance through the stack was then calculated using Ohm's law. In order to extract R_c, the resistance (R_{TE}) of a pure TE leg with the same geometry as the stack was measured in the same way. R_c was then determined using the following formula:

$$R_c = R_{TE/joint/TE} - R_{TE}. \tag{9.1}$$

The measurement was done at room temperature assuming there was no heat flux flowing through the material stack.

Mechanical Testing

Sample TE-legs of both N- and P-type material with Ti/Au metallization were sintered to both AlN/Cu and AlN/W substrates. The metallizations were identical to the hot side substrate metallization shown in Table 9.1.

The substrates were then mounted on a plate, which in turn was attached to one of the clamps in a MTS 20/M rig. On the other clamp, a hook was attached. The hook was placed on the surface of the TE-leg, as close to the substrate as possible without touching the surface. The clamps were then separated at a velocity of 1 mm/min and the force was recorded. Figure 9.2 shows a photograph of a substrate holding four TE-legs attached to the rig.

Results

R$_c$ *Measurement Results*

Table 9.2 shows the results from the R4P measurements of the joined TE-legs. The resistance through the stack ($R_{TE/joint/TE}$), resistivity (ρ), electrical conductivity (σ), and the resistance of the nano-Ag joints (R_c) are all derived from Equation 1. In addition, the TE-material properties were measured on TE-legs coming from the

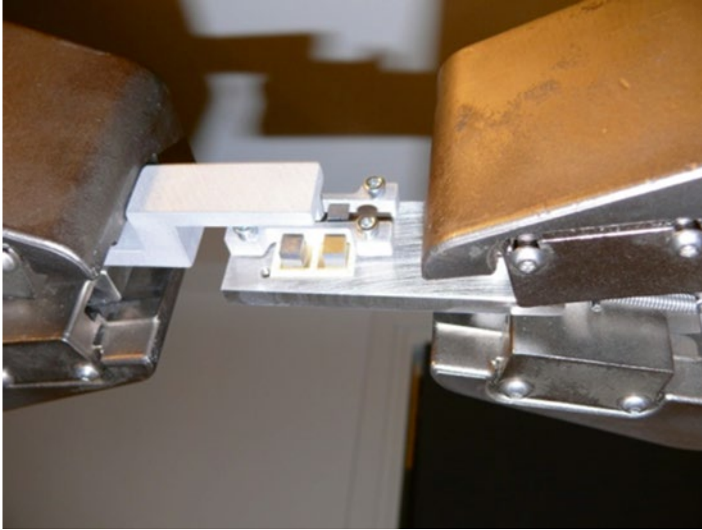

Fig. 9.2 A photograph of the shear test setup used in the MTS 20/M rig. A sample substrate with four TE-legs is mounted in the rig

same or similar pellets. In detail, the AA608P and AA786N material, both with Ti/Au metallization, showed low values of R_c. In one of the measurements, the stack became misaligned during the final pressure step of the sintering process (marked by * in Table 9.2) and should not be considered representative of the results. The measured $R_{TE/joint/TE}$ values were very high and dispersed for the AA637P and AA787N material stacks. The measured values were in the order of 300 times higher than R_{TE}, which results in the high R_c values derived.

Shear Test Results

Figure 9.3 shows shear diagrams for the AlN/Cu and AlN/W samples. For the AlN/Cu substrates, only two N-type material samples were tested successfully. The tests indicate a brittle fracture mechanism for the AlN/W, whilst the AlN/Cu samples experience some ductile behavior prior to fracture. Average shear strengths of 2.4 ± 1.4 MPa for the AlN/Cu substrate samples and 3.3 ± 1.9 MPa for the AlN/W substrate samples were obtained. For both substrate types, the results were largely dispersed.

An analysis of the fracture surfaces was done, which is shown in Fig. 9.4. It showed that the fracture surface contained mostly Ag for the AlN/Cu N2 sample while the AlN/W P1 sample fracture surface also included significant amounts of other elements. Au, Si, and Ge were easily identified in the spectrum.

Table 9.2 Results of the R_c measurements

SiGe legs with Nano-Ag			R4P Measurements			
TE material designation	Type	Metallization	$R_{TE/joint/TE}$ mΩ	ρ (μΩ·m)	σ (S/m)	R_c (Ω·m^2)
AA608	P	Ti/Au	2.5	12.4	80,336	–3.50E–10
			2.9	14.3	69,844	4.40E–09
			2.4	11.8	85,023	–2.10E–09
TE-material only (same pellet)				12.6	79,463	
AA637	P	$MoSi_2$/Ti/Ag	566.3	2780.3	360	7.10E–06
			18.3	89.9	11,123	2.00E–07
			576.8	2831.9	353	7.20E–06
TE-material only (similar pellet)				10.3	96,874	
AA786	N	Ti/Au	3.6	17.5	57,136	2.00E–09
			3.4	16.7	59,826	2.10E–09
			*5.1**	*25.1**	*39,858**	*2.10E–08**
TE-material only (similar pellet)				16.7	59,857	
AA787	N	$MoSi_2$/Ti/Ag	906.9	4452.5	225	1.10E–05
			688.8	3381.9	296	8.60E–06
			568.7	2792.1	358	7.10E–06
TE-material only (similar pellet)				16.7	59,857	

TEM Performance

AlN/Cu and AlN/W TEMs were tested on four probe setup to determine internal resistance at room temperature. The results are shown in Table 9.3. The TEMs built using AlN/W substrates had an internal resistance 2–3 times higher than the AlN/Cu samples.

Samples A1 and A2 in Table 9.3 subsequently failed during wiring, due to a faulty pressure application during the final sintering step, so they could not be used further in the performance tests. The AlN/W TEMs were tested under the following conditions:

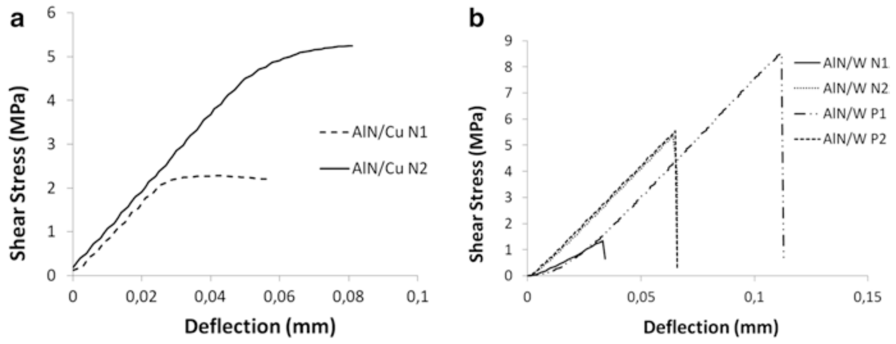

Fig. 9.3 Shear stress as a function of the actual movement of the shear tool. (**a**) Shows the results from the AlN/Cu substrates and (**b**) the results from the AlN/W substrates

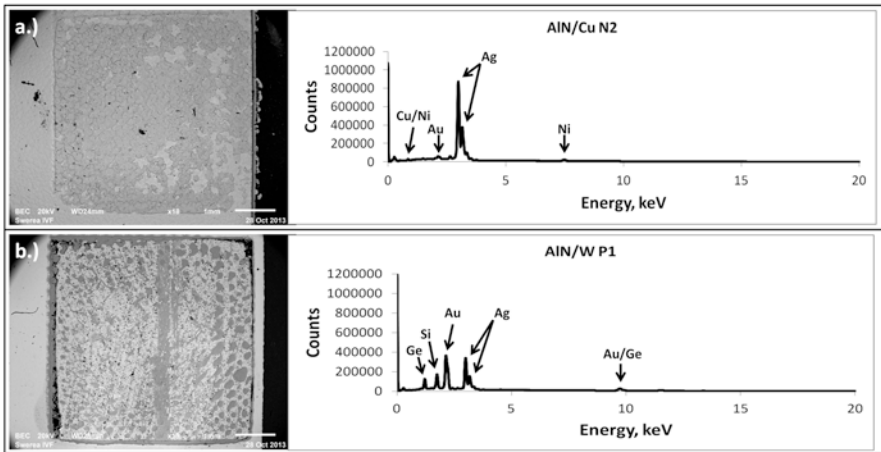

Fig. 9.4 SEM image and EDX spectral response of the shear test fracture surfaces of (**a**) AlN/Cu N2 and (**b**) AlN/W P1 samples

Table 9.3 Results of TEM resistance measurements

TEM	R4P (mΩ)
AlN/Cu—A1	11
AlN/Cu—A2	16
AlN/W—B1	32
AlN/W—B2	31

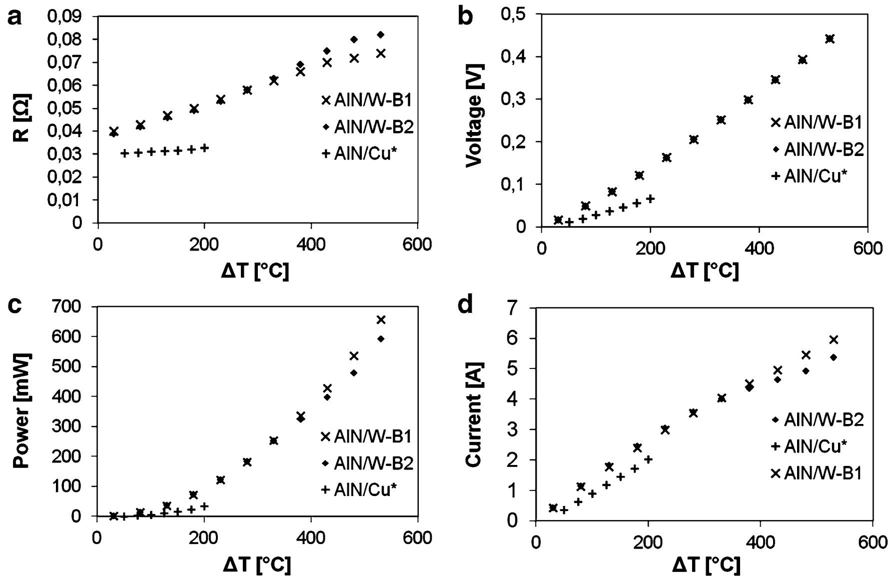

Fig. 9.5 Electrical results of the AlN/W TEMs. The figure shows (**a**) internal resistance, (**b**) open circuit voltage, (**c**) maximum power, and (**d**) current of the tested TEM

T cold: 20 °C
T hot: 50–550 °C
Pressure: 10 mBar

Figure 9.5 shows the electrical property measurements of the tested AlN/W TEMs. Measurements of current and power for AlN/Cu TEMs previously tested to 200 °C (denoted AlN/Cu*) have been included in Fig. 9.5 for comparison. A different connection technique was applied to the AlN/Cu* samples, with a 300 µm diameter Ag wires used to electrically connect the devices instead of the 300 µm thick Ag plates. The AlN/W devices tested resulted in higher values for all measurements except internal resistance, when compared to the AlN/Cu*devices.

Discussion of Results

The poor contact resistance from the $MoSi_2$/Ag metallization stack could be the result of inadequate cleaning of the SiGe surface prior to sputtering. There was also some miscoloration on the surface following the 900 °C anneal of unknown origin that could be linked to this. The future process will include Ar-plasma etch prior to the sputtering and a different furnace will be used for annealing.

In the shear tests, the AlN/W samples all displayed brittle behavior, whilst the AlN/Cu samples experienced some ductile behavior prior to fracture. This could be

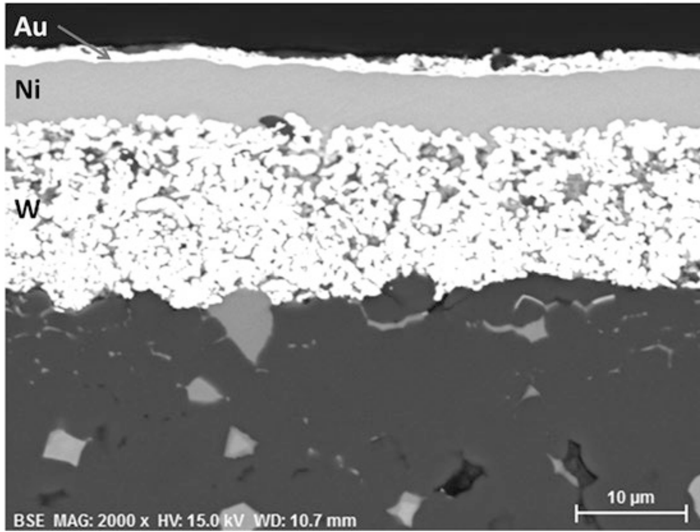

Fig. 9.6 Cross section SEM image of the AlN/W substrate metallization

an effect of the more ductile Cu (300 µm) compared to the W/Ni/Au metal stack (30 µm) on the substrate on which the TE-leg was attached. The analysis of the fracture surfaces in Fig. 9.4 showed almost exclusively Ag on the AlN/Cu fracture surface, while the AlN/W substrate also contained Au, Si, and Ge. This means that the fracture is located in the nano-Ag joint for the AlN/Cu substrates and in the interface between the SiGe TE-leg and the nano-Ag for the AlN/W substrate. Further analysis and better statistics are required.

The complete internal resistance of the AlN/Cu modules was almost 3 times lower than that of the AlN/W modules. This is mostly a result of the metallization thickness on the hot side substrates. The thickness of the AlN/Cu is 10 times thicker than for the AlN/W. Cu is also a better electrical conductor than W/Ni. This difference exists on both parts of metallization between the TE-legs and the hot side metallization which the current passes through. Additionally, as shown on the cross section image of the AlN/W substrate metallization in Fig. 9.6, the W layer is very porous, which increases the resistance further and it can be assumed that this layer has 60–80 % of the electrical conductivity of bulk W.

Figure 9.1 shows that the use of pressure in the sintering process significantly improves the density of the nano-Ag layer. Apart from mechanical consequences, this would also affect the electrical resistance. The AlN/Cu TEMs that failed after the internal resistance measurement could be expected to have even lower internal resistance when processed correctly.

The electrical results of the tested AlN/W TEMs are shown in Fig. 9.5. The internal resistance of sample B2 increases more than that for B1 with respect to temperature. The open circuit voltage is almost identical for both samples throughout the

entire temperature range. The AlN/W-B1 exhibits a slightly higher power output at higher temperatures, which is a result of the slightly higher current, which in turn results from a lower internal resistance for temperatures above 300 °C.

In spite of the lower performance of the AlN/Cu* sample, this version of the device still has a lower resistance than both AlN/W samples. This indicates that much improved results should be expected from the AlN/Cu versions with the new generation of TE-material when the correct pressure process is applied on these type of samples.

Conclusions

Results show that the use of nano-Ag sintered joints between TE-material and electrodes is possible, but the low and dispersed shear stress tolerance indicates there is room for improvement in the sintering process. The contact resistance of the nano-Ag layer was low in the case where the TE-leg metallization was Ti/Au. The low contact resistance was also reflected in the complete TEM measurements of the AlN/Cu substrate. The AlN/W TEMs show promising results, but they suffer from high internal resistance due to the thin metallization on the hot side substrates.

Acknowledgement This work was supported by the FP7 EU-project NEAT under grant agreement NMP4-SL-2011-263440.

References

1. Mondt, J. F., & Ambrus, J. H. (1984). Thermoelectric and thermionic conversion technology. NASA Conference Publication, 301–307.
2. Bennett, G. L., Lombardo, J. J., Hemler, R. J., Silverman, G., Whitmore, C. W., Amos, W. R., et al., (2008). The general-purpose heat source radioisotope thermoelectric generator: A truly general-purpose space RTG. AIP Conference Proceedings, 969: 663–671.
3. Ravi V, Firdosy S, Caillat T, Brandon E, Van Der Walde K, Maricic L et al (2009) J Electron Mater 38(7):1433–1442
4. Crane D, Lagrandeur J, Jovovic V, Ranalli M, Adldinger M, Poliquin E et al (2013) J Electron Mater 42(7):1582–1591
5. Schock H, Brereton G, Case E, D'Angelo J, Hogan T, Lyle M, et al (2013) J. Energy Resour. Technol. 135; JERT-11-1087; doi:10.1115/1.4023097
6. Roy G, Matagne E, Jacques PJ (2013) J Electron Mater 42(7):1781–1788
7. Wojciechowski KT, Zybala R, Mania R (2011) Microelectron Reliab 51:1198–1202
8. Fan J, Chen L, Bai S, Shi X (2004) Mater Lett 58:3876–3878
9. Zhao D, Li X, He L, Jiang W, Chen L (2009) Intermetallics 17:136–141
10. Zhao D, Tian C, Tang S, Liu Y, Jiang L, Chen L (2010) Mater Sci Semiconductor Process 13:221–224
11. Kadhim A, Hmood A, Abu Hassan H (2013) Mater Lett 97:24–26
12. Bai JG, Zhang ZZ, Calata JN, Lu G-Q (2004) IEEE Trans Compon Pack Technol. doi:10.1109/TCAPT.2005.853167

13. Chen G, Cao Y, Mei Y, Han D, Lu G-Q, Chen X (2012) IEEE Trans Compon Pack Manufact Technol 2(11):1759–67
14. Bernard-Granger G, Leforestier J, Navone C, Soulier M, Boidot M, Deniau B, et al (2013) “Microstructure–thermoelectrical properties relationships for a n-type polycrystalline Si1-xGex alloy sintered by SPS” Presented at the European-Materials Research Society Spring Meeting, May 27–30.
15. Inoue T, Koike K (1978) Appl Phys Lett 33:826
16. Cvitkovic R, Ivey DG, Stiles J (1995) J Mater Sci 30(21):5415–5426
17. Mochizuki T, Kashiwagi M (1980) J Electrochem Soc 127:1128